THE CONVECTIVE FLOW OF MAXWELL FLUID DRIVEN BY TWO ROTATING AND SPINNING DISKS

T. SINGLA, S. SHARMA and B. KUMAR†

School of Mathematics, Thapar Institute of Engineering and Technology, Patiala-147001, Punjab, India

Email: tanvisingla25@gmail.com, sapna.sharma@thapar.edu, chauhanbhuvan6@gmail.com

corresponding author†: chauhanbhuvan6@gmail.com

***Abstract* -- The present work addresses the axisymmetric flow of Maxwell fluid between two stretchable and rotating disks with porous regime. The influence of velocity slip and convective heat transfer are considered to govern the flow. The energy equation is modeled using Cattaneo-Christov heat flux model. The resulting mass, momentum and energy PDE's are converted to ODE's by using the Von Karman similarity transformations. Successive linearization method is implemented for numerical solution. The tangential velocity of the fluid increases with the rotating speed of the disks. The enhancement in the convective heat transfer of lower disc results in the rise of temperature profiles whereas temperature falls with the rise in Biot number of the upper disk. Moreover, by increasing porous permeability from 0.05 to 0.09, skin friction at lower disc is enhanced about 2.72%.**

***Keywords*- Maxwell fluid, Cattaneo-Christov model, Successive linearization Method, Convective flow, porous medium.**

I. INTRODUCTION

Rotating disk geometry is well known intriguing area in the field of fluid mechanics due to its outspread applications in power generation system, centrifugal filtration, aerodynamics, engine rotators, industrial and engineering sectors etc. Initially, the flow of Newtonian fluid over rotating disk was explored by Von Karman (1921) with constant angular velocity. He examined the solution by using the similarity approach. The numerical approach to solve fluid flow model over rotating disk was explored by Cochran (1934). After that, this model extension was done by Millsaps and Pohlhausen (1952) by incorporating the heat transfer characteristics. The flow and heat transfer properties over a rotating disk with magnetic field, porous media and radial electric effects was studied by Turkyilmazoglu (2012, 2016). Various non-Newtonian fluid flow models were discussed by Zaraki *et al*., 2015; Ellahi, 2018; Hayat *et al*., 2019; El-Zahar *et al*., 2021; Ali *et al*., 2022; Ejaz and Mustafa, 2022; Sharma *et al*., 2022; etc.

The non-Newtonian fluid flow models have made an impression on the mind of researchers due to its growing applications in chemical, polymer, petroleum, food processing industries etc. Various complex fluid flow processes are modeled in terms of non-Newtonian fluid model. Viscoelastic properties of fluid flow can also be examined using non-Newtonian fluid flow models. During past years, the researchers have engaged in the flow and heat transfer properties of Maxwell fluid due to its effectiveness for polymers of lower molecular weight. Abro *et al*. (2015) investigated the Maxwell fluid model to explain the viscoelastic property of the fluid having no-slip condition. The occurrence of heat transfer properties plays a major role in various scientific and industrial sectors like electronic, engine rotators, etc. Moreover, the induction of porous media also helps to enhance heat transfer properties (Ghalambaz *et al*., 2019; 2020). In recent times, Fourier (1878) proposed the Fourier law of heat conduction to study the heat transfer properties. It relates with parabolic kind of energy equation, whose influence is felt over the entire material.

Later the modification to this law was done by Cattaneo (1970) by introducing the new term 'thermal relaxation time' which increases the heat transfer process with finite speed. After that Christov (2009) again improved the Cattaneo's model by adding Oldroyd's upper convected derivative to the thermal relaxation time to obtain material invariant formulation. The behavior of Maxwell fluid over a stretched sheet using the Cattaneo–Christov heat flux model was examined by Hayat *et al.* (2015). He found that relaxation time parameter varies inversely with fluid temperature. Hayat *et al*. (2017) have taken Cattaneo-Christov heat flux model to study the heat transfer in the stagnation point flow of the fluid with temperature dependent thermal conductivity. Lim *et al*. (2021) studied the swirling flow problem for Casson fluid by taking Navier slip and the Cattaneo–Christov heat flux model. Wang *et al*. (2022a) explored buoyancy driven unsteady flow of Maxwell fluid via Cattaneo-Christov theory. Wang *et al.* (2022b) studied the Maxwell nanofluid flow with slip effects and convective boundary conditions over stretching surface. The dynamics of Maxwell fluid flow has been studied by various researchers like Ullah *et al*. (2017), Hayat and Sajid (2007), Abbas *et al*. (2006) and many others. Various magneto-fluid flow was discussed using Cattaneo–Christov heat flux model like (Reddy *et al.*, 2021, Jakeer *et al*., 2021).

Motivated by lots of applications of Maxwell fluid model in industrial and engineering sector, the prime objective of the work is to study the flow behavior of Maxwell fluid using Cattaneo-Christov heat flux model between two rotating and stretchable disks in the porous regime by assuming the velocity slip effects and convective heat transfer. The problem is modeled using three-dimensional momentum and energy equations and solved numerically using successive linearization method. The consequences of several involved parameters on axial, radial, tangential velocity and temperature profiles are depicted through graphs and discussed in detail.

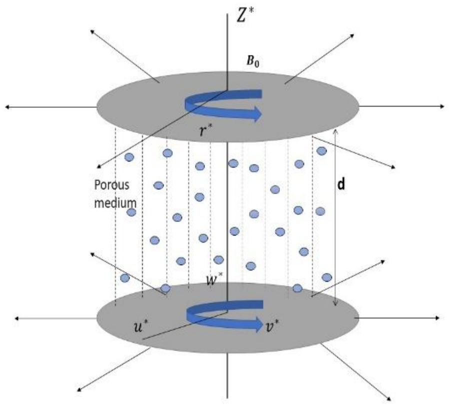

Figure 1:Schematics of the flow

II. MATHEMATICAL FORMULATION

We have considered steady, incompressible and axisymmetric Maxwell fluid flow between two co-axial, rotating and stretchable parallel disks. The cylindrical coordinated system is chosen as (r^*,θ^*,z^*). Velocity components are $V=[u^*(r^*,\theta^*,z^*), v^*(r^*,\theta^*,z^*), w^*(r^*,\theta^*,z^*)]$ ω_1 and ω_2 are the angular velocities of the lower and upper disk located at $z^*=0$ and $z^*=d$ as shown in Fig. 1. Let a_1 and a_2 are the stretching rates of lower and upper disks, respectively. Porous medium having permeability k_0 is considered in the model. The lower and upper disks are maintained at temperature T_1 and T_2, respectively. B_0 is the intensity of the magnetic field applied parallel to z^* axis.

The governing equations for Maxwell fluid model (Ahmed *et al*., 2020) can be written as:

$$\frac{\partial w^*}{\partial z^*}+\frac{\partial u^*}{\partial r^*}+\frac{u^*}{r^*}=0 \tag{1}$$

$$w^*\frac{\partial u^*}{\partial z^*}+u^*\frac{\partial u^*}{\partial r^*}-\frac{v^{*2}}{r^*}=\nu\left(-2\frac{u^*}{r^{*2}}+2\frac{\partial^2u^*}{\partial r^{*2}}+\frac{2}{r^*}\frac{\partial u^*}{\partial r^*}+\frac{\partial^2u^*}{\partial z^{*2}}+\frac{\partial^2w^*}{\partial r^*\partial z^*}\right)-\lambda_1\left(u^{*2}\frac{\partial^2u^*}{\partial r^{*2}}+\frac{v^{*2}u^*}{r^{*2}}-\frac{2u^*v^*}{r^*}\frac{\partial v^*}{\partial r^*}-\frac{2w^*v^*}{r^*}\frac{\partial v^*}{\partial z^*}+\frac{v^{*2}}{r^*}\frac{\partial u^*}{\partial r^*}+w^{*2}\frac{\partial^2u^*}{\partial z^{*2}}+2u^*w^*\frac{\partial^2u^*}{\partial r^*\partial z^*}\right)-\frac{1}{\rho}\frac{\partial p^*}{\partial r^*}-\frac{\sigma B_0^2}{\rho}\left(u^*+\lambda_1w^*\frac{\partial u^*}{\partial z^*}\right)-\frac{\nu}{k_0}u^* \tag{2}$$

$$w^*\frac{\partial v^*}{\partial z^*}+u^*\frac{\partial v^*}{\partial r^*}+\frac{v^*u^*}{r^*}=\nu\left(-\frac{v^*}{r^{*2}}+\frac{1}{r^*}\frac{\partial v^*}{\partial r^*}+\frac{\partial^2v^*}{\partial r^{*2}}++\frac{\partial^2v^*}{\partial z^{*2}}\right)-\lambda_1\left(u^{*2}\frac{\partial^2v^*}{\partial r^{*2}}-\frac{2u^{*2}v^*}{r^{*2}}-\frac{v^{*3}}{r^{*2}}+\frac{2w^*v^*}{r^*}\frac{\partial u^*}{\partial z^*}+\frac{v^{*2}}{r^*}\frac{\partial v^*}{\partial r^*}+2u^*w^*\frac{\partial^2v^*}{\partial r^*\partial z^*}+w^{*2}\frac{\partial^2v^*}{\partial z^{*2}}\right)-\frac{\sigma B_0^2}{\rho}\left(v^*+\lambda_1w^*\frac{\partial v^*}{\partial z^*}\right)-\frac{\nu}{k_0}v^* \tag{3}$$

$$w^*\frac{\partial w^*}{\partial z^*}+u^*\frac{\partial w^*}{\partial r^*}=\nu\left(\frac{\partial^2w^*}{\partial r^{*2}}+\frac{1}{r^*}\frac{\partial u^*}{\partial z^*}+\frac{1}{r^*}\frac{\partial w^*}{\partial r^*}+2\frac{\partial^2w^*}{\partial z^{*2}}+\frac{\partial^2u^*}{\partial r^*\partial z^*}\right)-\lambda_1\left(u^{*2}\frac{\partial^2w^*}{\partial r^{*2}}+\frac{v^{*2}}{r^*}\frac{\partial w^*}{\partial r^*}+w^{*2}\frac{\partial^2w^*}{\partial z^{*2}}+2u^*w^*\frac{\partial^2w^*}{\partial r^*\partial z^*}\right)-\frac{1}{\rho}\frac{\partial p^*}{\partial z^*}-\frac{\nu}{k_0}w^* \tag{4}$$

$$w^*\frac{\partial T^*}{\partial z^*}+u^*\frac{\partial T^*}{\partial r^*}=\frac{k}{(\rho c_p)}\left(\frac{\partial^2T^*}{\partial z^{*2}}+\frac{\partial^{*2}T^*}{\partial r^{*2}}+\frac{1}{r}\frac{\partial T^*}{\partial r^*}\right)-\gamma\left[u^{*2}\frac{\partial^2T^*}{\partial r^{*2}}+2u^*w^*\frac{\partial^2T^*}{\partial z^*\partial r^*}+w^{*2}\frac{\partial^2T^*}{\partial z^{*2}}+\left(w^*\frac{\partial u^*}{\partial z^*}+u^*\frac{\partial u^*}{\partial r^*}\right)\frac{\partial T^*}{\partial r^*}+\left(w^*\frac{\partial w^*}{\partial z^*}+u^*\frac{\partial w^*}{\partial r^*}\right)\frac{\partial T^*}{\partial z^*}\right] \tag{5}$$

The boundary conditions are: -

$$k\frac{\partial T^*}{\partial z^*}=-d_1(T_1-T^*),\ u^*=r^*a_1+\lambda_1^*\frac{\partial u}{\partial z},v^*=r^*\omega_1+\lambda_2^*\frac{\partial v}{\partial z},w^*=0 \text{ at } z^*=0, \tag{6}$$

$$k\frac{\partial T^*}{\partial z^*}=-d_2(T^*-T_2),u^*=r^*a_2-\lambda_1^*\frac{\partial u}{\partial z},v^*=r^*\omega_2-\lambda_2^*\frac{\partial v}{\partial z},w^*=0\ \text{ at } z^*=d, \tag{7}$$

where T^* is the fluid temperature, ν, B_0 , λ_1, ρ, σ is the kinematic viscosity coefficient, magnetic field strength, relaxation time, density, electrical conductivity of fluid, respectively. $d_1$and d_2 are the convective heat transfer coefficients at lower and upper disks respectively and (ρc_p), k is the heat capacitance and thermal conductivity of fluid. λ_2^* and λ_1^* are the velocity slip coefficients. γ is thermal relaxation time.

To solve the governing boundary layer Eqs. (2), (3), (4) and (5) along with boundary constraint (6) and (7), the following similarity transformations are used (Subbarayudu *et al*., 2019).

$$v^*=r^*\omega_1g(\eta),u^*=r^*\omega_1f'(\eta),w^*=-2d\omega_1f(\eta)$$
$$p^*=\rho\nu\omega_1\left(\frac{1}{2}\frac{r^{*2}}{d^2}\varepsilon+P(\eta)\right),\xi=\frac{z^*}{d},\theta(\eta)=\frac{T^*-T_2}{T_1-T_2}. \tag{8}$$

The Eqs. (2) - (5) transforms into the following forms:

$$f'''+\varepsilon-Re(f'^2-2ff''-g^2)+4Re\beta_1(ff'f''-f^2f'''-fgg')-MRe(f'-2\beta_1ff'')-\frac{1}{\beta}f'=0, \tag{9}$$

$$g''+2Re(-f'g+fg')+4Re\beta_1(-f^2g''+ff''g+ff'g')-MRe(g-2\beta_1fg')-\frac{1}{\beta}g=0, \tag{10}$$

$$P'+2f''+4Re(ff'-2\beta_1f^2f'')+\frac{2Re}{\beta}f=0, \tag{11}$$

$$\frac{1}{Pr}h''-4\lambda Re(ff'h'+f^2h'')+2Refh'=0. \tag{12}$$

The transformed boundary conditions are given below (Lim *et al*., 2021):

$$f'(0)=B_1+\gamma_1^*f''(0),f(0)=0,$$
$$\theta'(0)=-\gamma_1(1-\theta(0)),g(0)=1+\gamma_2^*g'(0),$$
$$f'(1)=B_2-\gamma_1^*f''(1),f(1)=0,$$
$$\theta'(1)=-\gamma_2\theta(1),P(0)=0,g(1)=\Omega-\gamma_2^*g'(1), \tag{13}$$

where $\beta_1=\lambda_1\omega_1$ is the Deborah number, $M=\frac{B_0^2\sigma}{\rho a_1}$, $\Omega=\frac{\omega_2}{\omega_1}$, $\beta=\frac{\omega_1k_0}{\nu}$ denotes magnetic parameter, rotation parameter, porosity parameter, respectively. $Re=\frac{\omega_1d^2}{\nu}$, $Pr=\frac{(\rho c_p)\nu}{k}$ denotes Reynolds number and Prandtl number, respectively. $B_2=\frac{a_2}{\omega_1}$ and $B_1=\frac{a_1}{\omega_1}$ are ratio of stretching rates to angular velocities, $\gamma_1=\frac{d_1d}{k}$ and $\gamma_2=\frac{d_2d}{k}$ are the thermal Biot numbers for lower and upper disk respectively. $\gamma_1^*=\frac{\lambda_1^*}{l}$ and $\gamma_2^*=\frac{\lambda_2^*}{l}$ stand for the velocity slip parameters for lower and upper disks respectively. $\lambda=\gamma\omega_1$ is thermal relaxation parameter.

On differentiating Eq. (9) w.r.t. η, we obtain-

$$f^{iv}-Re(-2ff'''-2gg')+4Re\beta_1(-ff'f'''+f'^2f''+ff''^2-f^2f^{iv}-f'gg'-fg'^2-fgg'')-MRe(f''-2\beta_1f'f''-2\beta_1ff''')-\frac{1}{\beta}f''=0. \tag{14}$$

The pressure parameter (ε) is given by:

$$\varepsilon=-f'''(0)+Re\left(f'^2(0)-2f''(0)f(0)-g^2(0)\right)-4Re\beta_1\left(f''(0)f'(0)f(0)-f'''(0)f^2(0)-f(0)g(0)g'(0)\right)$$

Table 1:Validation table for different values of Ω for non-stretching disk (Re = 1).

$\boldsymbol{\Omega}$	-0.3	0.0	0.50
$\boldsymbol{f''(0)}$			
Turkyilmazoglu (2016)	0.10395088	0.09997221	0.06663419
Present	0.10394983	0.09987695	0.06698356
$\boldsymbol{-g'(0)}$			
Turkyilmazoglu (2016)	1.30442355	1.00427756	0.50261351
Present	1.30489456	1.00427978	0.50268945

$$+\mathrm{MRe}(f'(0) - 2\beta_1 f''(0)f(0)) + \frac{1}{\beta}f'(0). \quad (15)$$

Shear stress in radial $(\tau_{z^*r^*})$ direction at lower rotating disk is:

$$\tau_{z^*r^*}\mu_f = \left.\frac{\partial u^*}{\partial z^*}\right|_{z^*=0} = \frac{\mu_f r^* \omega_1}{d} f''(0). \quad (16)$$

Shear stress in $(\tau_{z^*\theta})$ direction at lower rotating disk is:

$$\tau_{z^*\theta}\mu_f = \left.\frac{\partial v^*}{\partial z^*}\right|_{z^*=0} = \frac{\mu_f r^* \omega_1}{d} g'(0). \quad (17)$$

Total shear stress is defined by:

$$\tau_{w^*} = \sqrt{\tau_{z^*r^*}^2 + \tau_{z^*\theta}^2} =$$

$$\tau_{z^*\theta}\mu_f = \left.\frac{\partial v^*}{\partial z^*}\right|_{z^*=0} = \frac{\mu_f r^* \omega_1}{d} g'(0). \quad (17)$$

The local skin friction coefficients at the lower (C_1) and upper (C_2) disks are as follows: -

$$C_1 = \frac{\tau_{w^*}|_{z^*=0}}{\rho_f (r^*\omega_1)^2} = \frac{1}{\mathrm{Re}_{r^*}}\left[\left(f''(0)\right)^2 + \left(g'(0)\right)^2\right]^{1/2}, \quad (19)$$

$$C_2 = \frac{\tau_{w^*}|_{z^*=d}}{\rho_f (r^*\omega_2)^2} = \frac{1}{\mathrm{Re}_{r^*}}\left[\left(f''(1)\right)^2 + \left(g'(1)\right)^2\right]^{1/2}, \quad (20)$$

where $\mathrm{Re}_{r*} = \frac{r^*\omega_1 d}{\nu_f}$ represents the local Reynolds number.

III. SOLUTION METHODOLOGY

Successive linearization method (SLM) is utilized to solve Eqs. (10), (12) and (14) along with boundary conditions (13). The brief discussion of SLM working procedure is given in Kumar *et al.* (2019).

IV. VALIDATION OF NUMERICAL SOLUTION

To validate the numerical solution, we have adapted the model as per the work of Turkyilmazoglu (2016), i.e., by neglecting the effect of some parameters, $\beta_1 = 0$; M = 0, λ=0; $\gamma_1^* = 0$; $\gamma_2^* = 0$. Table 1 shows that our findings are agrees well with the data in the literature which confirms the accuracy of present analysis.

V. RESULTS AND DISCUSSION

This section involves the physical description of various involved parameters like Reynolds number (Re), Prandtl number (Pr), stretching parameters (B_1 and B_2), magnetic parameter (M), porous permeability parameter (β), rotation parameter (Ω), velocity slip parameters (γ_1^*, γ_2^*), thermal Biot numbers (γ_1, γ_2) on axial f (η) velocity, radial $f'(\eta)$ velocity, tangential $g(\eta)$ velocity and temperature $h(\eta)$ profiles are discussed. The values of some parameters are M = 1, Pr = 6.2, B_1 = 0.4, B_2= 0.5, Re = 0.7, λ = 0.5, γ_1 = 0.004, γ_2 = 0.006, β = 0.06, β_1 = 0.3, Ω = 0.9, $\gamma_1^* = 0.1$, $\gamma_2^* = 0.5$, until otherwise specified.

Figure 2 is plotted to determine the influence of stretching parameters (B_1 and B_2) on the axial velocity profile. The axial velocity profile shows the increasing trend with the rise in stretching rate of lower disk (B_1). For a particular value of B_1, the axial velocity shows the decreasing trend with inciting the value of B_2 due to the arise of centrifugal force.

Figure3 depicts the influence of porous parameter (β) and magnetic parameter (M) on the axial velocity profile. With rise in (β) from 0.03 to 0.09, axial velocity shows increasing trend near the vicinity of lower disk but it goes on decreasing while approaching towards the upper disk. Also, for particular value of β, it can be visualize that the axial velocity shows slight fall with rise in values of M near the end of the lower disk. After the inflection point ($\eta = 0.4$) nearly, the reverse trend can be seen near the upper disk. This can be attributed to the fact that a resistive force is created due to rise in magnetic field which hinders the motion of fluid particles.

Figure 4 reflects the radial velocity profile with the rise in streching parameters (B_1 and B_2). The dual behavior in the velocity profile is observed. The radial velocity also rises near the lower disk with the enhancement in its stretching rate. But it goes on decreasing when proceeds towards the upper disk. It can

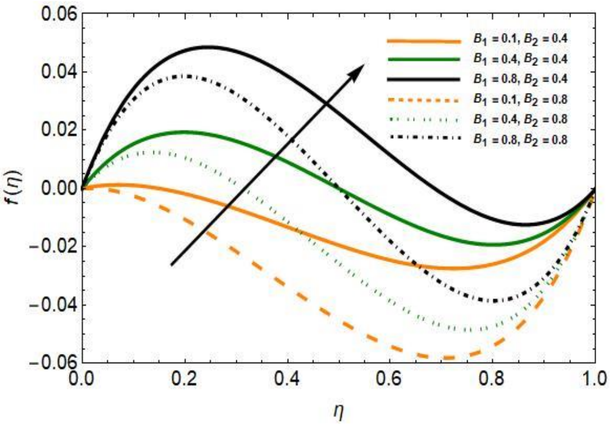

Figure 2: Axial velocity profiles for $B_1$and B_2.

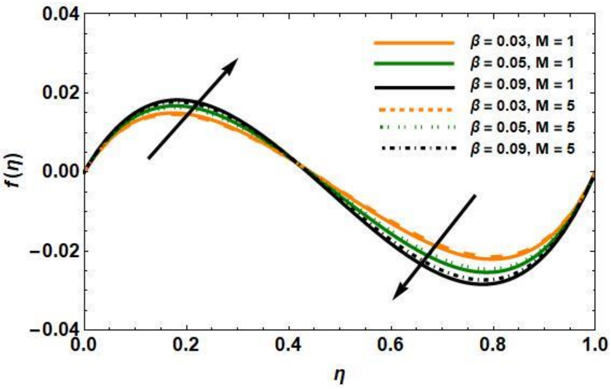

Figure3: Axial velocity profiles for β and M.

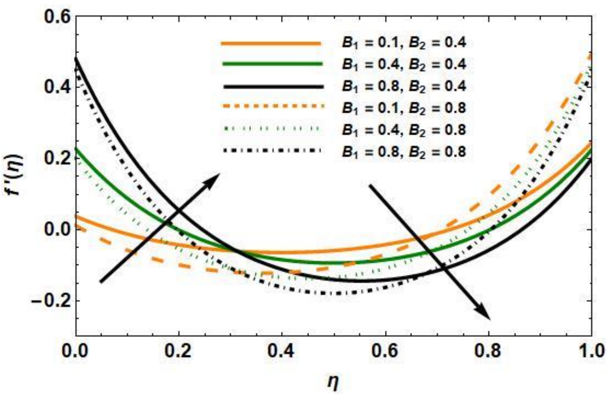

Figure 4: Radial velocity profiles for B_1 and B_2.

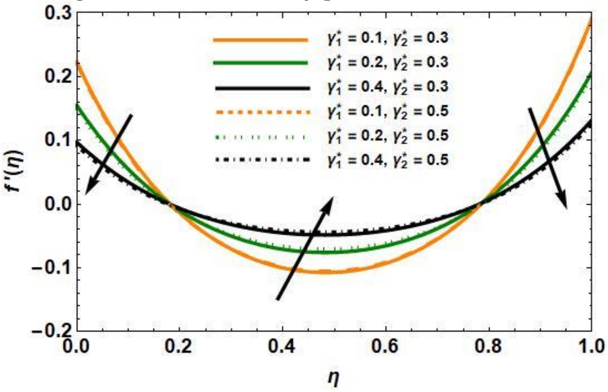

Figure 5: Radial velocity profiles for γ_1^* and γ_2^*.

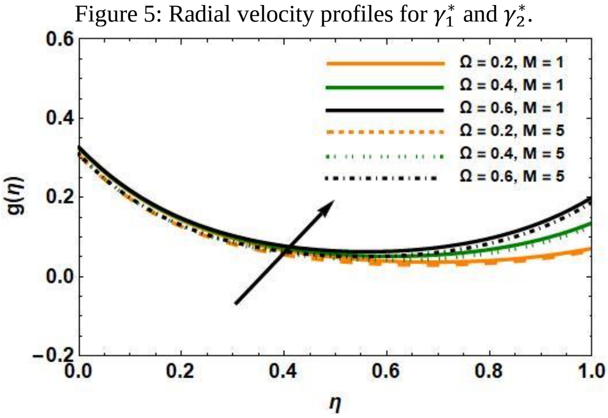

Figure 6: Tangential velocity profiles for M *and* Ω .

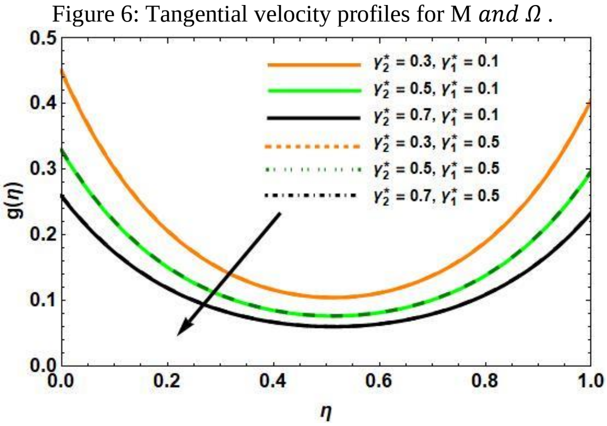

Figure 7: Tangential velocity profiles for γ_1^* and γ_2^*.

also be depicted from the figure that radial velocity profile increases near the vicinity of upper disk with the rise in the stretching rate (B_2) of upper disk.

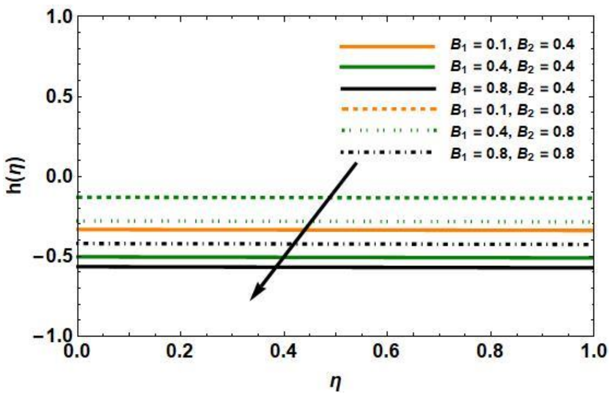

Figure 8: Temperature profile for $B_1 and\ B_2$.

Figure 5 contributes the influence of velocity slip parameters (γ_1^* and γ_2^*) on the radial velocity. The radial velocity falls near the ends of both disks with the enhancement in slip paramerters. But it shows increasing trend in the mid section of the flow domain. From the graph, two points of inflection nearly at 0.2 and 0.8 are captures.

Figure is plotted to visualize the trend of tangential velocity profile due to rotation parameter (Ω) and magnetic parameter (M). From the expression $\Omega = \frac{\omega_2}{\omega_1}$, it can be seen that rise in Ω means rotation speed of upper disk will be more than that of lower disk. So tangential velocity shows an increasing trend and more fluid will flow from the slow moving disk to the faster moving disk. Magnetic parameter (M) somewhat hinders the fluid motion, that's why velocity is observed to be slightly less because of rise in M.

In Figure , the profile of tangential velocity is drawn on varying velocity slip parameters (γ_1^* and γ_2^*). The rise in velocity slip γ_2^* results in the decline of tangential velocity profile. Both γ_1^* and γ_2^* cause reduction in velocity trend.

Figure 8 captures the influence of stretching parameters (B_1 and B_2) on the temperature distribution of fluid flow. From Fig. 8, it is clear that the fall in temperature profile is observed due to increase in stretching rate of lower disk. Whereas, with enhancement in B_2, the temperature profile shows an increasing trend. Centripital force account for this occurrence.

Figure determines the impact of Prandtl number (Pr) and Reynolds number (Re) on the temperature profile of fluid. High values of Re accounts for less viscosity of the fluid. So the rise in the values of Re results in enhancement of temperature of fluid. Large values of Pr means that the thermal diffusivity of the fluid is low. Also, Fig. 9 shows that the temperature of the fluid rises with rise in Pr.

Figure is plotted to notice the behavior of thermal Biot numbers $\gamma_1 and\ \gamma_2$ on the temperature of fluid. Biot numbers are related with convective heat transfer coefficients due to lower and upper disks. When heat transfer coefficient of lower disk enhances, temperature of fluid also rises. But when there is more heat transfer at the vicinity of upper disk then fall in temperature profile is observed.

Table 2: Skin friction variation for different parameters

Re	Pr	Ω	B_1	B_2	β	M	γ_1	γ_2	γ_1^*	γ_2^*	Re_rC_1	Re_rC_2
0.5	3	0.2	0.1	0.2	0.03	1	0.002	0.004	0.1	0.3	2.18012	0.980895
0.7											2.18236	0.982221
0.9											2.18459	0.983538
0.5	5										2.18012	0.980895
	7										2.18012	0.980895
	3	0.4									2.17924	1.22362
		0.6									2.17751	1.90929
		0.2	0.4								2.76287	1.11573
			0.8								4.049	1.29888
			0.1	0.4							2.20507	1.77472
				0.8							2.26667	3.42661
				0.2	0.05						1.97994	0.895488
					0.09						1.7425	0.808453
					0.03	5					2.20245	0.991408
						7					2.21309	0.996486
						1	0.004				2.18012	0.980895
							0.008				2.18012	0.980895
							0.002	0.006			2.18012	0.980895
								0.008			2.18012	0.980895
								0.004	0.5		2.12493	0.526897
									0.7		2.12192	0.484033
									0.1	0.5	1.57488	0.934468
										0.7	1.25758	0.915322

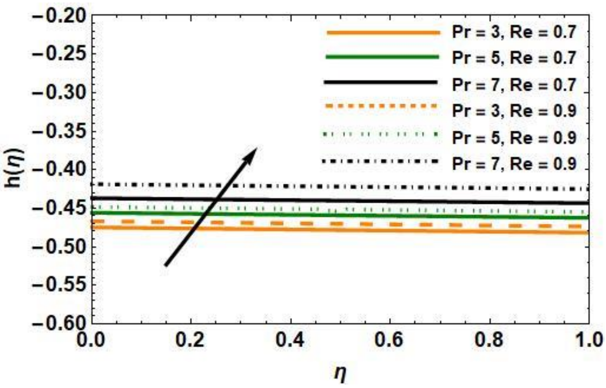

Figure 9: Temperature profiles for Pr and Re.

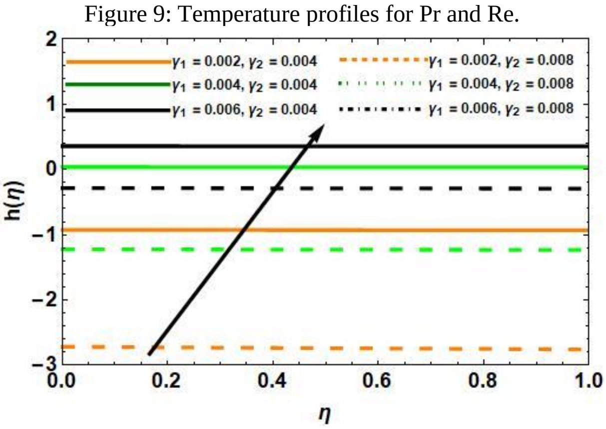

Figure 10: Temperature profiles for γ_1 and γ_2.

Table 2 shows the skin friction coefficient for various involved parameters. Skin friction arises due to movement of fluid layers one over the other. Different parameters have different contribution in creating friction among the fluid layers. From Table 2, it is clear that skin friction increases with increase in Reynolds number because viscous forces rises with Re. The Prandtl number has almost no effect on the value of skin friction coefficient. Skin friction coefficient near the lower disk falls when the rotation speed of lower disk is more whereas it rises with increase in rotation speed of upper one. When the stretching rate of lower disk and upper disk extends, skin friction coefficient accelerates near the ends of both the disks. Under the influence of porous medium, skin friction falls with rise in porosity parameter. Thermal Biot numbers has negligible impact on the skin friction values. The skin friction coefficient drops with the rise in velocity slip near the vicinity of both the disks.

VI. CONCLUSIONS

The current study deals with Maxwell fluid confined between two stretchable and rotating disks with the porous media and multiple slips. The physical description of various involved parameters like Reynolds number (Re), stretching rates (B_1 and B_2), magnetic parameter (M), Prandtl number (Pr), porous permeability parameter (β), velocity slip parameters (γ_1^*, γ_2^*), rotation parameter (Ω), thermal Biot numbers (γ_1, γ_2) on axial f (η) velocity, radial $f'(\eta)$ velocity, tangential $g(\eta)$ velocity and temperature $h(\eta)$ profiles are discussed. Some of the main finding of the present study includes:

- The axial velocity of fluid accelerates with the rise in stretching rate of lower disk whereas it retards when the stretching rate of upper disk rises. The centrifugal force accounts for this occurrence.
- The rotation parameter boosts the tangential velocity profile up because of elevation in relative speeds of both disks.
- The velocity slip parameters exhibit more elevation in tangential velocity and skin friction near both the discs.

- The rise in thermal Biot numbers of the lower and upper disk results in enhancement and decay of fluid temperature respectively.
- The porosity parameter and slip parameters reduce the skin friction at both discs. By increasing porous permeability from 0.05 to 0.09, skin friction at lower disc is enhanced about 2.72%.

NOMENCLATURE

u^*, v^*, w^*	Velocity components
T^*	Temperature
B_0	Magnetic field strength
M	Magnetic parameter
Re	Reynolds number
Pr	Prandtl number
B_1, B_2	Stretching parameter
ρ	Density
k	Thermal conductivity
ρc_p	Heat capacitance
k_0	Porosity of porous regime
f, f', g	Axial, radial, tangential velocity

Greek symbols

$\lambda_2^*,\ \lambda_1^*$	Velocity slip coefficients
γ	Thermal relaxation time
ν	Kinematic viscosity
σ	Electrical conductivity
λ_1	Relaxation time
β_1	Deborah number
Ω	Rotation parameter
β	Porosity parameter
γ_1, γ_2	Thermal Biot numbers
γ_1^*, γ_2^*	Velocity slip parameters
λ	Thermal relaxation parameter
τ	Shear stress

REFERENCES

Abbas, Z., Sajid, M. and Hayat, T. (2006) MHD boundary-layer flow of an upper-convected Maxwell fluid in a porous channel. *Theoretical and Computational Fluid Dynamics*. **20**, 229-238.

Abro, K.A., Shaikh, A.A., Junejo, I.A. and Chandio, M.S. (2015) Analytical solutions under no slip effects for accelerated flows of Maxwell fluids. *Sindh University Research Journal-SURJ (Science Series)*. **47,** 11.

Ahmed, J., Khan, M. and Ahmad, L. (2020) Effectiveness of homogeneous–heterogeneous reactions in Maxwell fluid flow between two spiraling disks with improved heat conduction features. *Journal of Thermal Analysis and Calorimetry*. **139**, 3185-3195.

Ali, U., Irfan, M., Rehman, K.U., Alqahtani, A. S., Malik, M.Y., & Shatanawi, W. (2022) On the Cattaneo–Christov heat flux theory for mixed convection flow due to the rotating disk with slip effects. *Waves in Random and Complex Media*, 1-15.

Cattaneo, C. (1970) *On the conduction of heat*. US Department of Commerce, Technology Administration, National Technical Information Service.

Christov, C.I. (2009) On frame indifferent formulation of the Maxwell–Cattaneo model of finite-speed heat conduction. *Mechanics Research Communications.* **36**, 481-486.

Cochran, W.G. (1934) The flow due to a rotating disk *Mathematical proceedings of the Cambridge philosophical society*. **30**, 365-375.

Ejaz, I. and Mustafa, M. (2022) A comparative study of different viscosity models for unsteady flow over a decelerating rotating disk with variable physical properties. *International Communications in Heat and Mass Transfer*. **135**, 106155.

Ellahi, R., Zeeshan, A., Hussain, F. and Abbas, T. (2018) Study of shiny film coating on multi-fluid flows of a rotating disk suspended with nano-sized silver and gold particles: A comparative analysis. *Coatings*. **8**, 422.

El-Zahar, E.R., Mahdy, A.E.N., Rashad, A.M., Saad, W. and Seddek, L.F. (2021) Unsteady MHD mixed convection flow of non-Newtonian Casson hybrid nanofluid in the stagnation zone of sphere spinning impulsively. *Fluids*, ***6***(6), 197.

Fourier, J.B.J. (1878) *The analytical theory of heat*. The University Press.

Ghalambaz, M., Noghrehabadi, A., Chamkha, A. and Nadeem, S. (2020) Analytical solution of free convection heat transfer of hybrid nanofluids over a vertical flat plate embedded in a porous medium. *Mathematical Methods in the Applied Sciences*.

Ghalambaz, M., Groşan, T. and Pop, I. (2019) Mixed convection boundary layer flow and heat transfer over a vertical plate embedded in a porous medium filled with a suspension of nano-encapsulated phase change materials. *Journal of Molecular Liquids*. **293**, 111432.

Hayat, T. and Sajid, M. (2007) Homotopy analysis of MHD boundary layer flow of an upper-convected Maxwell fluid. *International Journal of Engineering Science*. **45**, 393-401.

Hayat, T., Farooq, M., Alsaedi, A. and Al-Solamy, F. (2015) Impact of Cattaneo-Christov heat flux in the flow over a stretching sheet with variable thickness. *Aip Advances*. **5**, 087159.

Hayat, T., Haider, F., Muhammad, T. and Ahmad, B. (2019) Darcy–Forchheimer flow of carbon nanotubes due to a convectively heated rotating disk with homogeneous–heterogeneous reactions. *Journal of Thermal Analysis and Calorimetry*. **137**, 1939-1949.

Hayat, T., Khan, M.I., Waqas, M. and Alsaedi, A. (2017) On Cattaneo–Christov heat flux in the flow of variable thermal conductivity Eyring–Powell fluid. *Results in Physics*. **7**, 446-450.

Jakeer, S., Reddy, P.B., Rashad, A.M. and Nabwey, H.A. (2021) Impact of heated obstacle position on magneto-hybrid nanofluid flow in a lid-driven porous cavity with Cattaneo-Christov heat flux pattern. *Alexandria Engineering Journal*. **60**, 821-835.

Kumar, B., Seth, G.S. and Nandkeolyar, R. (2019) Successive linearisation approach to analyse thermally radiative stagnation point micropolar nanofluid flow with regression model. *Pramana - J Phys*. **93**, 74.

Lim, Y.J., Zakaria, M.N., Isa, S. M., Zin, N. A. M., Mohamad, A. Q., & Shafie, S. (2021) Von Kármán Casson fluid flow with Navier's slip and cattaneo-christov heat flux. *Case Studies in Thermal Engineering*. **28**, 101666.

Millsaps, K. and Pohlhausen, K. (1952) Heat transfer by laminar flow from a rotating plate. *Journal of the Aeronautical Sciences*. **19**, 120-126.

Reddy, S.R.R., Reddy, P.B.A. and Rashad, A.M. (2021) Effectiveness of binary chemical reaction on magneto-fluid flow with Cattaneo–Christov heat flux model. *Proceedings of the Institution of Mechanical Engineers, Part C: Journal of Mechanical Engineering Science*. **235**, 2192-2200.

Sharma, K., Kumar, S. and Vijay, N. (2022) Numerical simulation of MHD heat and mass transfer past a moving rotating disk with viscous dissipation and ohmic heating. *Multidiscipline Modeling in Materials and Structures*.

Subbarayudu, K., Suneetha, S., Bala Anki Reddy, P. and Rashad, A.M. (2019) Framing the activation energy and binary chemical reaction on CNT's with Cattaneo–Christov heat diffusion on Maxwell nanofluid in the presence of nonlinear thermal radiation. *Arabian Journal for Science and Engineering.* **44**, 10313-10325.

Turkyilmazoglu, M. (2012) Effects of uniform radial electric field on the MHD heat and fluid flow due to a rotating disk. *International Journal of Engineering Science*. **51**, 233-240.

Turkyilmazoglu, M. (2016) Flow and heat simultaneously induced by two stretchable rotating disks. *Physics of Fluids*. **28**, 043601.

Ullah, H., Islam, S., Khan, I., Bin Shafie, S. and Fiza, M. (2017) MHD boundary layer flow of an incompressible upper convected Maxwell fluid by Optimal Homotopy Asymptotic Method. *Scientia Iranica*. **24**, 202-210.

Von Kármán, T. (1921) Uber laminare und turbulente Reibung. *Z. Angew. Math. Mech.* **1**, 233-252.

Wang, F., Ahmed, A., Naveed Khan, M., Alqahtani, T., and Algarni, S. (2022a) Features of energy transfer in buoyancy-driven unsteady flow of Maxwell fluid via Cattaneo–Christov theory. *Waves in Random and Complex Media*, 1-15.

Wang, F., Ahmad, S., Al Mdallal, Q., Alammari, M., Khan, M.N. and Rehman, A. (2022b) Natural bioconvective flow of Maxwell nanofluid over an exponentially stretching surface with slip effect and convective boundary condition. *Scientific Reports*. **12**, 1-14.

Zaraki, A., Ghalambaz, M., Chamkha, A. J., Ghalambaz, M. and De Rossi, D. (2015) Theoretical analysis of natural convection boundary layer heat and mass transfer of nanofluids: effects of size, shape and type of nanoparticles, type of base fluid and working temperature. *Advanced Powder Technology*. **26**, 935-946.

Received: July 16, 2022
Sent to Subject Editor: August 29, 2022
Accepted: January 21, 2023
Recommended by Subject Editor Gianfranco Caruso